ACS APPLIED ELECTRONIC MATERIALS

pubs.acs.org/acsaelm

Article

Tuning Ionic Conductivity in Fluorite Gd-Doped CeO_2-Bixbyite RE_2O_3 (RE = Y and Sm) Multilayer Thin Films by Controlling Interfacial Strain

Gene Yang, Mohammad El Loubani, Habib Rostaghi Chalaki, Jiwon Kim, Jong K. Keum, Christopher M. Rouleau, and Dongkyu Lee*

Cite This: *ACS Appl. Electron. Mater.* 2023, 5, 4556−4563

Read Online

ACCESS | Metrics & More | Article Recommendations | Supporting Information

ABSTRACT: Interfacial strain in heteroepitaxial oxide thin films is a powerful tool for discovering properties and recognizing the potential of materials performance. Particularly, facilitating ion conduction by interfacial strain in oxide multilayer thin films has always been seen to be a highly promising route to this goal. However, the effect of interfacial strain on ion transport properties is still controversial due to the difficulty in deconvoluting the strain contribution from other interfacial phenomena, such as space charge effects. Here, we show that interfacial strain can effectively tune the ionic conductivity by successfully growing multilayer thin films composed of an ionic conductor Gd-doped CeO_2 (GDC) and an insulator RE_2O_3 (RE = Y and Sm). In contrast to compressively strained GDC-Y_2O_3 multilayer films, tensile strained GDC-Sm_2O_3 multilayer films demonstrate the enhanced ionic conductivity of GDC, which is attributed to the increased concentration of oxygen vacancies. In addition, we demonstrate that increasing the number of interfaces has no impact on the further enhancement of the ionic conductivity in GDC-Sm_2O_3 multilayer films. Our findings demonstrate the unambiguous role of interfacial strain on ion conduction of oxides and provide insights into the rational design of fast ion conductors through interface engineering.

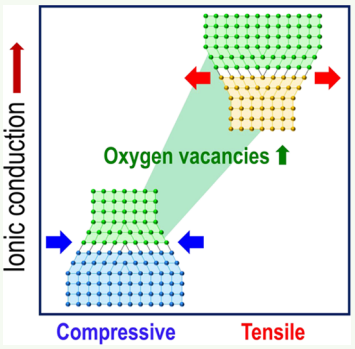

KEYWORDS: *interfacial strain, pulsed laser deposition, epitaxial strain-induced ionic conductivity, oxide multilayer thin films, fluorite structure, bixbyite oxide structure*

1. INTRODUCTION

Achieving fast ion transport at reduced temperatures is a key requirement to develop advanced oxide-based energy applications, including solid oxide fuel cells,[1,2] batteries,[3,4] oxygen permeable membranes,[5] and catalysts.[6] In recent years, with the development of thin film technologies, such as pulsed laser deposition (PLD), growing attention has been directed toward investigating ion conduction in oxide thin film heterostructures, where tuning interfacial strain is known as a control knob for altering the migration of oxygen ions[7−10] and the formation of oxygen vacancies[11−15] at heterointerfaces.

In oxide thin film heterostructures, strain can be introduced into heterointerfaces via lattice mismatch.[14] However, by increasing the lattice mismatch and film thickness, the interface can change from coherent to incoherent as dislocations are introduced to relieve strain.[10] Appropriate lattice mismatch and film thickness (a few nanometers thick) are thus essential for obtaining suitable strain levels (∼±3%) to elucidate the interfacial strain effect on ion conduction. However, ultrathin films exhibit extremely large resistance, which makes the choice of substrate critical to avoid the substrate shunt current from dominating the transport. To accurately and reliably evaluate the oxygen ion conductivity, it is necessary to use insulating substrates, such as Al_2O_3, MgO, and $NdGaO_3$ (NGO).[16−18] Despite their insulating properties, such substrates generally cause a large lattice mismatch with oxide thin films, resulting in poor crystallinity of the films, which, in turn, hampers the identification of the strain effect on ion conduction.

Furthermore, depending on the combination of materials, it is difficult to deconvolute the strain contribution from multiple factors, such as space charge layers (SCLs), to the ionic conductivity in multilayer thin films. For example, in the case of undoped ionic conductors with a low intrinsic defect concentration, such as CeO_2, creating a heterointerface with insulating oxides enabled the enhancement of the ionic conductivity of CeO_2 due to the formation of SCLs.[19] Heterointerfaces between two different doped ion conductors, such as a lateral multilayer composed of Sm-doped CeO_2 (SDC) and Y-doped ZrO_2 (YSZ),[20] also enhanced the ionic

Received: May 30, 2023
Accepted: July 23, 2023
Published: August 4, 2023

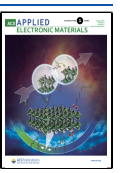

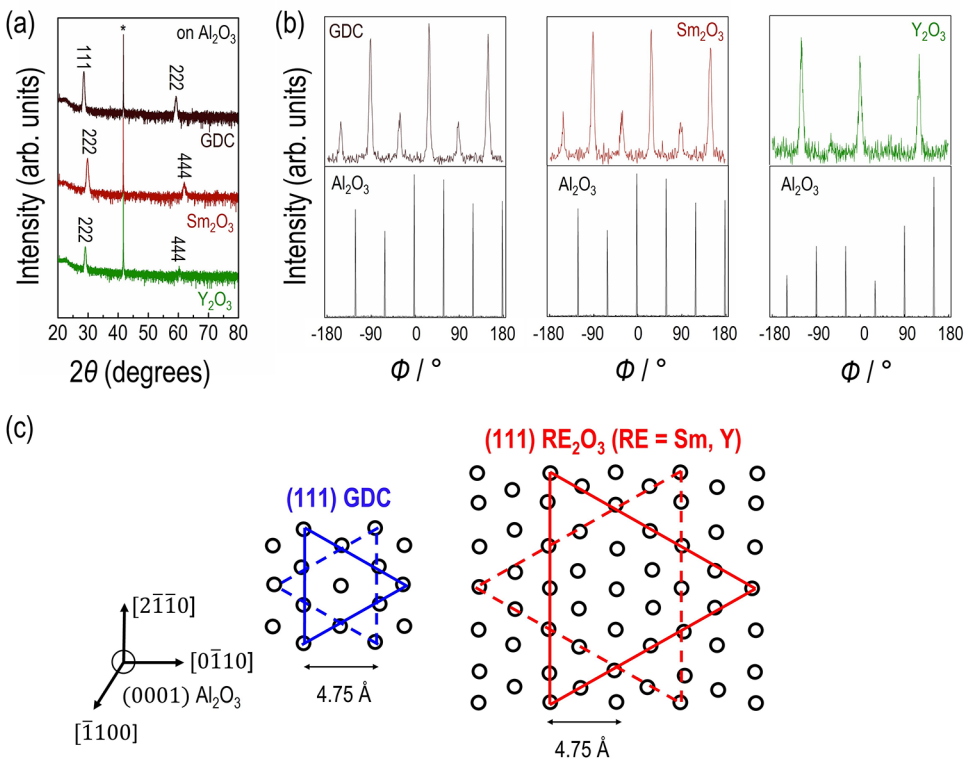

Figure 1. (a) XRD θ–2θ patterns of the epitaxial single layer GDC, Sm_2O_3, and Y_2O_3 films grown on Al_2O_3 substrates. (b) XRD ϕ scans of the 113 reflections of Al_2O_3 substrate, 200 reflections of GDC film, and 400 reflections of RE_2O_3 (RE = Y and Sm). (c) Schematic illustration of in-plane lattice matching based on XRD θ–2θ patterns and ϕ scans (black circles represent oxygens of Al_2O_3).

conductivity without the formation of SCLs, which were likely negligible anyway due to the large intrinsic defect concentrations.[10] However, due to the simultaneous contribution of two ionic conductors to the total conductivity, deconvoluting the strain contribution to the total conductivity was impossible.

As a result of such difficulties noted in these material systems and limited appropriate substrates, the effect of strain on enhancing the ionic conductivity is still quite controversial.[10,20−23] What is needed to explore the effect of strain on ion conduction is a precise synthesis of high-quality multilayer thin films on insulating substrates and the careful selection of material systems. In particular, an ionic conductor with abundant oxygen vacancies and an insulator are needed to exclude the SCLs and the contribution to the ionic conductivity, respectively. In addition, the lattice mismatch between these materials should be in the range of ∼±2% to form a coherent interface. To meet these requirements, a combination of fluorite Gd-doped CeO_2 (GDC) and bixbyite RE_2O_3 (RE = Y and Sm) is a promising material combination.

In this work, we present the effect of strain on ionic conductivity by successfully creating heterointerfaces composed of an ionic conductor GDC and an insulator RE_2O_3 (RE = Y and Sm) grown on insulating Al_2O_3 substrates. Considering the lattice mismatch between fluorite GDC and bixbyite RE_2O_3 (RE = Y and Sm), Sm_2O_3 (a = 10.935 Å),[24] and Y_2O_3 (a = 10.604 Å)[25] introduce tensile (∼1.1%) and compressive (∼−2%) strain, respectively, into GDC (a = 5.410 Å).[26] The interfacial strain is modulated by controlling the thickness of each layer in epitaxial GDC-RE_2O_3 multilayer thin films on Al_2O_3. In contrast to compressive strain, tensile strain results in an increase in the oxygen vacancy concentration, which, in turn, leads to the enhanced ionic conductivity of GDC. This work demonstrates that controlling interfacial strain in multilayer thin films is a simple and effective means to tune the ionic conductivity of oxides.

2. EXPERIMENTAL DETAILS

2.1. Synthesis of GDC-RE_2O_3 (RE = Y and Sm) Multilayer Films. Epitaxial GDC-RE_2O_3 (RE = Y and Sm) multilayer films with different thicknesses of GDC (∼5, ∼10, ∼30, and ∼50 nm) were grown by PLD on single-crystal (0001) Al_2O_3 substrates. To achieve the desired strain in the GDC films, the thickness of the RE_2O_3 layers was consistently set at 100 nm on Al_2O_3 substrates to ensure their relaxation state. The substrates were attached to the PLD substrate holder using a small amount of silver paint for thermal contact. PLD was performed using a KrF excimer laser at λ = 248 nm, 10 Hz pulse rate, and ∼1 J/cm^2 fluence under an oxygen partial pressure, $p(O_2)$, of 1.3 × 10^{-4} atm (100 mTorr) at 700 °C. After completing the deposition, the samples were cooled to room temperature in the PLD chamber for 1 h under a $p(O_2)$ of 1.3 × 10^{-4} atm (100 mTorr).

2.2. Characterization of Physical and Chemical Properties. Oxide phase purity and crystallography of the films were investigated via high-resolution X-ray diffraction (HRXRD) using a four-circle diffractometer. Measurements were performed using in-plane and out-of-plane configurations. The thicknesses of the films were characterized by X-ray reflectivity (XRR) measurements. *In situ* HRXRD was performed on a four-circle diffractometer in a $p(O_2)$ of 1 atm and a controlled temperature stage (DHS 900, Anton Paar). Silver paste was used to adhere the thin film sample to the heating plate. The heating rate was ∼10 °C min^{-1}, and the temperature was held for 20 min at each temperature (25 and 700 °C) before XRD data were collected. Sample realignment was conducted at each temperature to maximize the XRD intensities. A full range θ–2θ normal scan was collected, and then high-resolution θ–2θ normal scans of GDC (111) and Al_2O_3 (0002) were collected. As the thermocouple for this experiment was placed inside the heating stage, a small difference between the set and actual temperatures on the

https://doi.org/10.1021/acsaelm.3c00724
ACS Appl. Electron. Mater. 2023, 5, 4556−4563

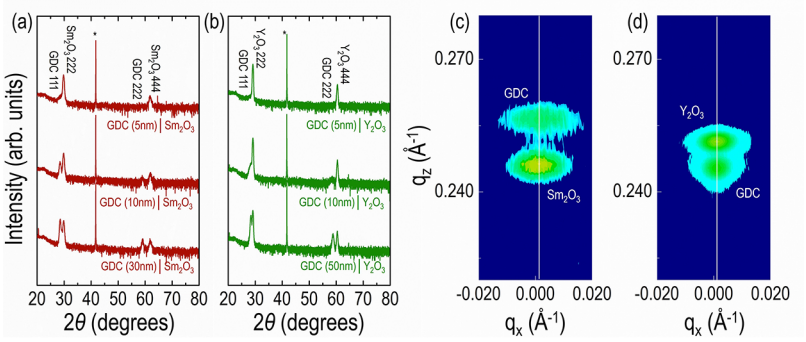

Figure 2. XRD θ–2θ patterns of the epitaxial (a) GDC-Sm_2O_3 and (b) GDC-Y_2O_3 multilayer films grown on Al_2O_3 substrates. X-ray reciprocal space maps (RSMs) of the (c) tensile strained GDC-Sm_2O_3 and (d) compressively strained GDC-Y_2O_3 multilayer films.

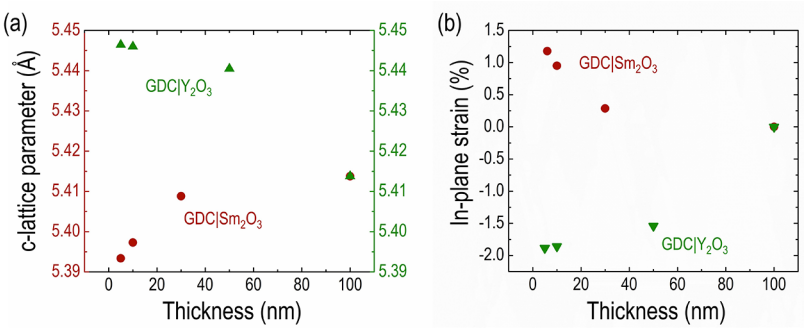

Figure 3. Changes of (a) *c*-axis lattice parameter and (b) in-plane strain of GDC extracted from GDC-RE_2O_3 (RE = Y and Sm) multilayer films as a function of GDC thickness.

sample surface cannot be excluded. Raman scattering measurements were performed with an Xplora plus Raman spectrometer. A 50× magnification long working distance (8 mm) objective was used with a laser excitation wavelength of 638 nm. The Raman spectra were collected using the LabSpec 6 software every 1 min.

2.3. Evaluation of Ionic Conductivity. To measure the ionic conductivity of the GDC single layer and GDC-RE_2O_3 (RE = Y and Sm) multilayer films, in-plane dc measurements were performed with a source meter (Keithley 2450) in a two-electrode configuration geometry using silver paste electrodes painted onto the film surface. The dc measurements were carried out at a temperature of 450 to 700 °C. The dc measurements were also performed while varying the oxygen partial pressure $p(O_2)$ from 10^{-3} to 1 atm.

3. RESULTS AND DISCUSSION

3.1. Crystallinity of the Epitaxial GDC-RE_2O_3 (RE = Y and Sm) Multilayer Films. Prior to the synthesis of multilayer thin films, the growth of single layer films was required to optimize the growth conditions for each layer. XRD θ–2θ scans shown in Figure 1 confirmed that GDC and RE_2O_3 (RE = Sm and Y) single layer films were grown epitaxially. The films showed only (hhh) peaks, indicating (111)-oriented films on (0001) Al_2O_3. The ϕ scans of the GDC and RE_2O_3 (RE = Sm and Y) single layer films showed that (200) GDC, (400) RE_2O_3 (RE = Sm and Y), and (113) Al_2O_3 have strong peaks with 6-fold symmetry (Figure 1b), which reveals the in-plane crystallographic relationships between GDC, RE_2O_3 (RE = Sm and Y) and Al_2O_3 (in-plane 30° rotation). According to the 6-fold symmetry of the (0001) Al_2O_3 and 3-fold symmetry of the (111) GDC and RE_2O_3 (RE = Sm and Y),[27] single layers of GDC and RE_2O_3 (RE = Sm and Y) could be deposited on (0001) Al_2O_3 with the following epitaxy relationship: (111) GDC or (111) RE_2O_3||(0001) Al_2O_3 and $[\bar{1}10]$ GDC or $[\bar{1}10]$ RE_2O_3||$[\bar{1}10]$ Al_2O_3, $[1\bar{1}0]$ GDC or $[1\bar{1}0]$ RE_2O_3||$[\bar{1}10]$ Al_2O_3 (Figure 1c). The deposition of GDC and RE_2O_3 (RE = Sm and Y) with a 3-fold symmetry can be achieved in two different directions on (0001) Al_2O_3, resulting in the 6-fold symmetry observed in the ϕ scans (Figure 1b). It is worth noting that epitaxial Sm_2O_3 thin films were successfully grown on Al_2O_3. In fact, despite the advantages of using Sm_2O_3 as a counterpart material in oxide multilayer films, the growth of epitaxial Sm_2O_3 films is difficult compared to that of other rare-earth oxides,[28,29] which, in turn, leads to the limited range of strain that can be induced by the lattice mismatch with other oxides.

Based on the optimized growth conditions of single layers, epitaxial GDC-RE_2O_3 (RE = Sm and Y) multilayer films were deposited on Al_2O_3 (Figure 2). The films clearly show the presence of only (hhh) peaks of GDC and RE_2O_3 (RE = Sm and Y), indicating that the films grew epitaxially. To precisely control the interfacial strain, the thickness of GDC was carefully modulated in the nanometer range, which was a challenge in this study. One concern could be the cation diffusion between the GDC and RE_2O_3 during film deposition and ionic conductivity measurements. However, previous studies already reported that there was no cation interdiffusion between fluorite CeO_2 and bixbyite RE_2O_3 due to the extremely low diffusion coefficients of rare-earth cations in CeO_2 at 650 °C and below.[19,30,31] XRD reciprocal space maps (RSMs) around the 103 Bragg reflections of the Al_2O_3 indicate that Sm_2O_3 and Y_2O_3 introduced in-plane tensile and compressive strain, respectively, into GDC (Figure 2c,d).

3.2. Strain in the Epitaxial GDC-RE_2O_3 (RE = Y and Sm) Multilayer Films. The systematic change in the c-axis lattice constant of GDC was observed as the thickness of GDC decreased in the GDC-RE_2O_3 (RE = Sm and Y) multilayer films, leading to the change in the in-plane lattice strain of

https://doi.org/10.1021/acsaelm.3c00724
ACS Appl. Electron. Mater. 2023, 5, 4556−4563

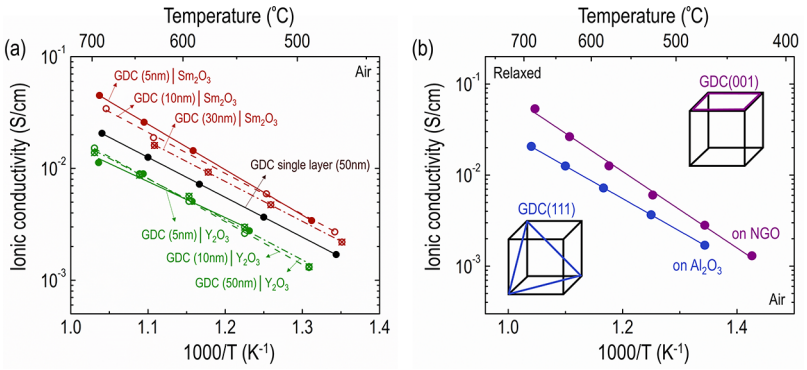

Figure 4. Temperature dependence of the ionic conductivity of (a) GDC-RE_2O_3 (RE = Sm and Y) multilayer films. The ionic conductivity of GDC single layer (relaxed) is also plotted for comparison. (b) Ionic conductivity comparison between (111)- and (001)-oriented GDC films.

GDC due to the Poisson's ratio (Figure 3a). The in-plane lattice strain of GDC in the GDC-RE_2O_3 (RE = Sm and Y) multilayer films is shown in Figure 3b. The in-plane strain of GDC increased as the GDC thickness decreased. The GDC film with a thickness of ∼5 nm on Sm_2O_3 was found to have a strain of ∼1.2%, whereas the same thickness of GDC on Y_2O_3 resulted in a strain of −1.9%. For GDC thicknesses less than 50 nm, a negligible change in compressive strain was observed compared to the tensile GDC-Sm_2O_3 case. This trend implies that the compressive strain induced at a GDC thickness of ∼50 nm has already reached the theoretical compressive strain calculated from the bulk lattice parameters of GDC and Y_2O_3.[25,26] These strain calculations based on changes in the in-plane lattice parameter of GDC are in good agreement with the RSMs discussed in Figure 2.

3.3. Ionic Conductivity of the Epitaxial GDC-RE_2O_3 (RE = Y and Sm) Multilayer Films. As discussed earlier, careful attention should be paid to the selection of substrates and counterpart materials to access the ionic conductivity of oxide multilayer thin films. If the counterpart materials or substrates have comparable resistance with the materials under study, then the measured ionic conductivity can be attributed to all components. Therefore, the resistance from the substrate and RE_2O_3 (RE = Sm and Y) without the GDC thin film layer should be confirmed to be at least 1 order of magnitude lower than that of the GDC thin film for meaningful measurements.[32,33] In this study, we confirmed that the ionic conductivities of the substrates and RE_2O_3 (RE = Sm and Y) were at least 3 orders of magnitude lower than that of bulk GDC (Figure S1).[34] In addition, the resistances of the substrates and RE_2O_3 were more than 1 order of magnitude larger than that of the GDC thin films.

Figure 4a shows the Arrhenius plots of the conductivity measured in the temperature range of 450 to 750 °C in air for the GDC-RE_2O_3 (RE = Sm and Y) multilayer films, as well as the strain-relaxed GDC single layer as a reference deposited epitaxially on Al_2O_3. The ionic conductivity of the GDC-RE_2O_3 (RE = Sm and Y) multilayer films did not change with oxygen partial pressure. This result indicates that the conductivity of the GDC-RE_2O_3 (RE = Sm and Y) multilayer films was attributed to the ionic conductivity within our test range (Figure S2).[35] An increase in the ionic conductivity of GDC by tensile strain in the GDC-Sm_2O_3 multilayer films was observed. By decreasing the thickness of GDC in the GDC-Sm_2O_3 multilayer films, the tensile strain increased, resulting in an approximate twofold enhancement in the ionic conductivity of GDC compared to a GDC single layer. While the strain-enhanced ionic conductivity was not significant, the enhancement in the in-plane ionic conductivity of doped ionic conductors by lattice strain is generally less than 1 order of magnitude due to the structural limitations for coherency strain.[10,20,23,36−41] Interestingly, decreasing the GDC thickness resulted in a slight increase in the activation energy from 0.7 to 0.8 eV, which is mainly attributed to the distortion of the strained lattice.[33,42,43] The GDC-Y_2O_3 multilayer films with compressive strain exhibited a reduction in the ionic conductivity, resulting in an approximate twofold decrement compared to a GDC single layer. However, for GDC-Y_2O_3 multilayer films with a GDC thickness below ∼50 nm, the compressive strain did not significantly affect ionic conductivity and activation energy, which is consistent with the observation of negligible changes in compressive strain with varying GDC thickness as discussed in Figure 3b.

3.4. Effect of Crystallographic Orientations on Ionic Conductivity. In addition to tuning epitaxial strain, controlling crystallographic orientations of oxides can be another promising approach to enhance ionic conductivity since oxygen transport and defect formation energies can be altered depending on the crystallographic orientations.[44,45] The orientation of epitaxial films is mainly dependent upon that of the substrates. In contrast to single-crystal (0001) Al_2O_3, which resulted in strained (111)-oriented epitaxial GDC films, strain-relaxed, (001)-oriented epitaxial GDC films were grown on single-crystal (110) NGO substrates (Figure S3). Details about the XRD analysis of (001)-oriented epitaxial GDC films can be found in the Supporting Information. We confirmed that the conductivity of the (001)-oriented GDC film was dominated by an ionic contribution within our tests (Figure S4). Interestingly, as shown in Figure 4b, the ionic conductivity of the (001)-oriented GDC film was higher than that of the (111)-oriented GDC film, most likely due to the different migration paths for oxygen vacancies that vary with the crystallographic plane.[33,44,46] This result is further supported by the fact that the activation energy required for the migration of oxygen vacancies is lower in the ⟨001⟩ direction than in the ⟨111⟩ direction.[44] Consequently, controlling the in-plane strain in (001)-oriented GDC films is expected to result in enhanced ionic conductivity compared to the (111)-oriented GDC films,[46] but further studies are needed to confirm this hypothesis.

3.5. Influence of the Number of Strained Interfaces on Ionic Conductivity. As discussed earlier, the structural limitations for coherency strain constrain the enhancement of the in-plane ionic conductivity of GDC. To overcome such

https://doi.org/10.1021/acsaelm.3c00724
ACS Appl. Electron. Mater. 2023, 5, 4556−4563

limitations, increasing the number of strained interfaces by synthesizing oxide superlattices can be an approach.[47,48] While oxide superlattices have shown great promise for creating unique materials properties,[49−54] the effect of the increased number of interfaces on ionic conductivity is still under debate.[20,22,47,48,55] To systematically investigate the effect of the number of interfaces on ionic conductivity, superlattices of $[(GDC)_1|(Sm_2O_3)_1]_n$, where n is the number of GDC-Sm_2O_3 bilayers, were successfully synthesized with n equal to 1, 3, 6, and 20. The presence of distinct satellite peaks in the XRD θ–2θ pattern for n = 20 indicates the characteristic features of a superlattice structure (Figure S5), signifying the presence of well-defined and high-quality interfaces between the two constituent oxides.[20,22] To keep the same amount of tensile strain on the GDC film, we only changed the number of layers and fixed the GDC thickness at 5 nm. Interestingly, no significant difference in the ionic conductivity was shown by increasing the number of interfaces from 1 to 20 (Figure 5).

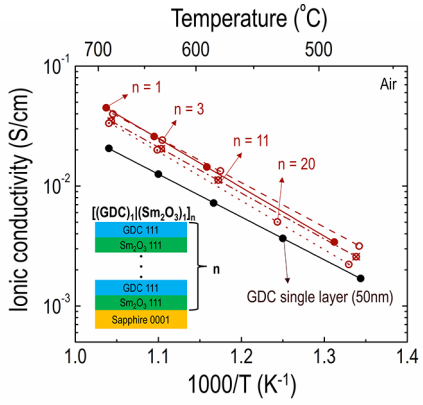

Figure 5. Temperature dependence of the ionic conductivity of $[(GDC)_1|(Sm_2O_3)_1]_n$ superlattices. The ionic conductivity of the GDC single layer (relaxed) is also plotted for comparison.

This observation confirms that the number of interfaces does not play a crucial role in determining the ionic conductivity of $[(GDC)_1|(Sm_2O_3)_1]_n$ superlattices, which is consistent with other studies.[22,55] A plausible explanation for ionic conductivity that is independent of the number of interfaces may be made by considering the geometric constraints of planar thin films. Specifically, as the total thickness of the superlattice increases, the interfaces can be degraded due to the formation of misfit dislocations. Ultimately, this degradation can result in incoherent interface structures, which adversely affect the ionic conductivity of the system.[55,56] This hypothesis can be supported by a slight decrease in the ionic conductivity when n = 20 in the $[(GDC)_1|(Sm_2O_3)_1]_n$ superlattices. Furthermore, the activation energies of the superlattices, ranging from 0.7 to 0.8 eV, were found to be randomly distributed without exhibiting a distinct trend. Further studies are needed to see if controlling the thickness of each layer to retain coherent interface structures can further enhance the ionic conductivity of $[(GDC)_1|(Sm_2O_3)_1]_n$ superlattices.

3.6. Relation between Oxygen Vacancy Concentration and Strain. Tensile strain is generally known to decrease the energy required for the formation of oxygen vacancies, increasing the concentration of oxygen vacancies.[7,15] This increase in oxygen vacancies is a major contributor to increased ionic conductivity in oxides.[57,58] In order to examine the change of oxygen vacancies depending on strain, *in situ* HRXRD measurements were performed. Here, we calculated the unit cell volumes of GDC-RE_2O_3 (RE = Sm and Y) multilayer films because the unit cell volume of GDC changes with varying concentrations of oxygen vacancies.[45,59] Based on the results of the temperature-dependent unit cell volume (Figure 6a), we calculated the thermal expansion coefficient (TEC) of the GDC single layer and GDC-RE_2O_3 (RE = Sm and Y) multilayer films (2.4×10^{-5}–3.1×10^{-5} °C^{-1}), which were found to be comparable with the previously reported GDC bulk TEC[60] (1.25×10^{-5} °C^{-1}). The unit cell volume of the GDC-Sm_2O_3 multilayer film under tensile strain was observed to be larger than that of the GDC single layer. Conversely, the unit cell volume of the GDC-Y_2O_3 multilayer film under compressive strain was found to be smaller. This observation strongly indicates that tensile strain promotes an increase in the concentration of oxygen vacancies, while compressive strain has the opposite effect, reducing their concentration. The increased oxygen vacancies by tensile strain are further supported by the results of Raman spectroscopy measurements (Figure 6b). The peak of the tensile strained GDC-Sm_2O_3 multilayer film shifted to lower energy and became broader compared to relaxed GDC single layer and compressively strained GDC-Y_2O_3 multilayer film. Previous

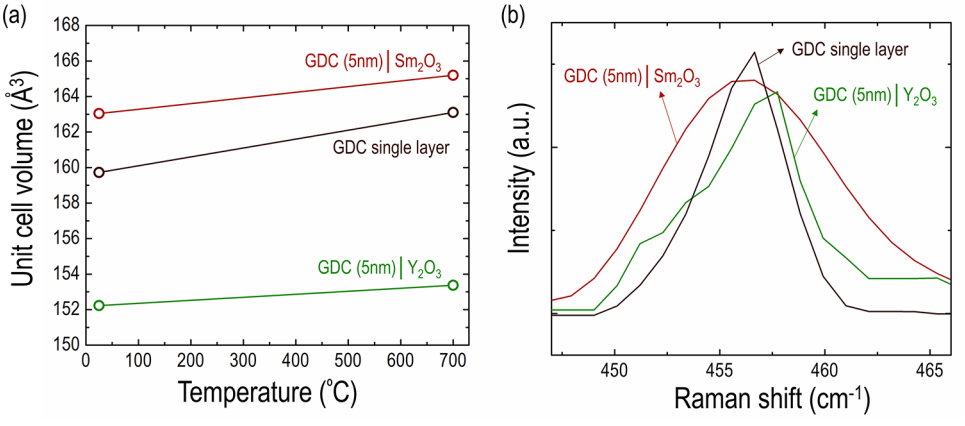

Figure 6. (a) Unit cell volume change as a function of temperature of GDC-RE_2O_3 (RE = Sm and Y) multilayer films and GDC single layer obtained from *in situ* HRXRD measured from 25 to 700 °C in air. (b) Raman peak shift of GDC-RE_2O_3 (RE = Sm and Y) multilayer films and GDC single layer obtained from Raman spectroscopy measurements.

https://doi.org/10.1021/acsaelm.3c00724
ACS Appl. Electron. Mater. 2023, 5, 4556−4563

studies demonstrated a similar trend in the peak shift to lower Raman energy and broadening with increased oxygen vacancy concentration in GDC.[61,62] Thus, our *in situ* HRXRD and Raman spectroscopy measurements confirmed that the increased concentration of oxygen vacancies resulting from tensile strain in GDC-RE_2O_3 (RE = Sm and Y) multilayer films can enable enhanced ionic conductivity.

4. CONCLUSIONS

In summary, we successfully synthesized multilayer thin films composed of ionic conducting GDC and insulating rare-earth oxides RE_2O_3 (RE = Y and Sm), demonstrating the unambiguous effect of strain on ionic conductivity. Compared to compressively strained GDC-Y_2O_3 multilayer films, tensile strained GDC-Sm_2O_3 multilayer films exhibited improved ionic conductivity. The creation of more oxygen vacancies induced by tensile strain, as confirmed by *in situ* HRXRD and Raman spectroscopy results, was responsible for the enhancement of ionic conductivity. However, there was no significant difference in the ionic conductivity by increasing the number of interfaces in GDC-Sm_2O_3 superlattices. We also showed that (001)-oriented GDC films were beneficial for enhancing ionic conductivity compared to (111)-oriented GDC films. Our results highlight the importance of properly designing oxide multilayers to identify the interfacial strain effect on ionic conductivity and the potential of forming coherent interfacial strain to tune the ionic conductivity.

■ ASSOCIATED CONTENT

Supporting Information

The Supporting Information is available free of charge at https://pubs.acs.org/doi/10.1021/acsaelm.3c00724.

Ionic conductivity measurements and high-resolution X-ray diffraction (HRXRD) (PDF)

■ AUTHOR INFORMATION

Corresponding Author

Dongkyu Lee − *Department of Mechanical Engineering, University of South Carolina, Columbia, South Carolina 29208, United States;* orcid.org/0000-0003-4700-5047; Email: dongkyu@cec.sc.edu

Authors

Gene Yang − *Department of Mechanical Engineering, University of South Carolina, Columbia, South Carolina 29208, United States*

Mohammad El Loubani − *Department of Mechanical Engineering, University of South Carolina, Columbia, South Carolina 29208, United States*

Habib Rostaghi Chalaki − *Department of Mechanical Engineering, University of South Carolina, Columbia, South Carolina 29208, United States*

Jiwon Kim − *Department of Mechanical Engineering, University of South Carolina, Columbia, South Carolina 29208, United States*

Jong K. Keum − *Center for Nanophase Materials Sciences, Oak Ridge National Laboratory, Oak Ridge, Tennessee 37830, United States*

Christopher M. Rouleau − *Center for Nanophase Materials Sciences, Oak Ridge National Laboratory, Oak Ridge, Tennessee 37830, United States*

Complete contact information is available at: https://pubs.acs.org/10.1021/acsaelm.3c00724

Author Contributions

G.Y.: Methodology, investigation, formal analysis, visualization, writing—original draft; M.E.L.: Methodology, investigation, writing—review and editing; H.R.C.: Investigation, writing—review and editing; J.K.: Investigation, writing—review and editing; J.K.K.: Visualization, writing—review and editing; C.M.R.: Synthesis environment, visualization, writing—review and editing; D.L.: Supervision, conceptualization, methodology, writing—review and editing.

Funding

This research was funded by the U.S. Department of Energy (DOE), Office of Science (OS), Basic Energy Sciences (BES), grant number DE-SC0021363, and National Science Foundation (grant number 2110033).

Notes

The authors declare no competing financial interest.

■ ACKNOWLEDGMENTS

Film synthesis and *in situ* HRXRD measurements were conducted as part of a user project at the Center for Nanophase Materials Sciences (CNMS), which is a US Department of Energy, Office of Science User Facility at Oak Ridge National Laboratory.

■ REFERENCES

(1) Shao, Z. P.; Haile, S. M. A High-performance Cathode for the Next Generation of Solid-oxide Fuel Cells. *Nature* **2004**, *431*, 170−173.

(2) Wachsman, E. D.; Lee, K. T. Lowering the Temperature of Solid Oxide Fuel Cells. *Science* **2011**, *334*, 935−939.

(3) Dunn, B.; Kamath, H.; Tarascon, J. M. Electrical Energy Storage for the Grid: A Battery of Choices. *Science* **2011**, *334*, 928−935.

(4) Tarascon, J. M.; Armand, M. Issues and Challenges Facing Rechargeable Lithium Batteries. *Nature* **2001**, *414*, 359−367.

(5) Hendriksen, P. V.; Larsen, P. H.; Mogensen, M.; Poulsen, F. W.; Wiik, K. Prospects and Problems of Dense Oxygen Permeable Membranes. *Catal. Today* **2000**, *56*, 283−295.

(6) Voskresenskaya, E. N.; Roguleva, V. G.; Anshits, A. G. Oxidant Activation Over Structural Defects of Oxide Catalysts in Oxidative Methane Coupling. *Catal. Rev.* **1995**, *37*, 101−143.

(7) De Souza, R. A.; Ramadan, A.; Hörner, S. Modifying the Barriers for Oxygen-vacancy Migration in Fluorite-structured CeO_2 Electrolytes Through Strain: A Computer Simulation Study. *Energy Environ. Sci.* **2012**, *5*, 5445−5453.

(8) Lee, D.; Lee, H. Controlling Oxygen Mobility in Ruddlesden−Popper Oxides. *Materials* **2017**, *10*, No. 368.

(9) Rupp, J. L. M. Ionic Diffusion as a Matter of Lattice-strain for Electroceramic Thin Films. *Solid State Ionics* **2012**, *207*, 1−13.

(10) Korte, C.; Peters, A.; Janek, J.; Hesse, D.; Zakharov, N. Ionic Conductivity and Activation Energy for Oxygen Ion Transport in Superlattices-The Semicoherent Multilayer System YSZ (ZrO_2 + 9.5 mol% Y_2O_3)/Y_2O_3. *Phys. Chem. Chem. Phys.* **2008**, *10*, 4623−4635.

(11) Guo, X. X.; Maier, J. Ionically Conducting Two-Dimensional Heterostructures. *Adv. Mater.* **2009**, *21*, 2619−2631.

(12) Morgan, D.; Mayeshiba, T. (Invited) Ab Initio Studies of Strain Effects on Perovskite Oxygen Vacancy Formation and Migration Energetics. *ECS Meet. Abstr.* **2016**, *MA2016-01*, No. 1489.

(13) Lee, D.; Jacobs, R.; Jee, Y.; Seo, A.; Sohn, C.; Ievlev, A. V.; Ovchinnikova, O. S.; Huang, K.; Morgan, D.; Lee, H. N. Stretching Epitaxial $La_{0.6}Sr_{0.4}CoO_{3-\delta}$ for Fast Oxygen Reduction. *J. Phys. Chem. C* **2017**, *121*, 25651−25658.

(14) Herklotz, A.; Lee, D.; Guo, E. J.; Meyer, T. L.; Petrie, J. R.; Lee, H. N. Strain Coupling of Oxygen Non-stoichiometry in Perovskite Thin Films. *J. Phys.: Condens. Matter* **2017**, *29*, No. 493001.

(15) Aidhy, D. S.; Liu, B.; Zhang, Y. W.; Weber, W. J. Strain-Induced Phase and Oxygen-Vacancy Stability in Ionic Interfaces from First-Principles Calculations. *J. Phys. Chem. C* **2014**, *118*, 30139−30144.
(16) Zhang, Y. W.; Jin, S.; Yang, Y.; Li, G. B.; Tian, S. J.; Jia, J. T.; Liao, C. S.; Yan, C. H. Electrical Conductivity Enhancement in Nanocrystalline $(RE_2O_3)_{0.08}(ZrO_2)_{0.92}$ (RE = Sc, Y) Thin Films. *Appl. Phys. Lett.* **2000**, *77*, 3409−3411.
(17) Kim, S. M.; Son, J. W.; Lee, K. R.; Kim, H.; Kim, H. R.; Lee, H. W.; Lee, J. H. Substrate Effect on the Electrical Properties of Sputtered YSZ Thin Films for Co-planar SOFC Applications. *J. Electroceram.* **2010**, *24*, 153−160.
(18) Chen, L.; Chen, C.; Huang, D.; Lin, Y.; Chen, X.; Jacobson, A. High Temperature Electrical Conductivity of Epitaxial Gd-doped CeO_2 Thin Films. *Solid State Ionics* **2004**, *175*, 103−106.
(19) Shen, W.; Jiang, J.; Ni, C.; Voras, Z.; Beebe, T. P.; Hertz, J. L. Two-dimensional Vacancy Trapping in Yttria Doped Ceria. *Solid State Ionics* **2014**, *255*, 13−20.
(20) Sanna, S.; Esposito, V.; Tebano, A.; Licoccia, S.; Traversa, E.; Balestrino, G. Enhancement of Ionic Conductivity in Sm-doped Ceria/Yttria-stabilized Zirconia Heteroepitaxial Structures. *Small* **2010**, *6*, 1863−1867.
(21) Garcia-Barriocanal, J.; Rivera-Calzada, A.; Varela, M.; Sefrioui, Z.; Iborra, E.; Leon, C.; Pennycook, S. J.; Santamaria, J. Colossal Ionic Conductivity at Interfaces of Epitaxial ZrO_2: Y_2O_3/$SrTiO_3$ Heterostructures. *Science* **2008**, *321*, 676−680.
(22) Pergolesi, D.; Fabbri, E.; Cook, S. N.; Roddatis, V.; Traversa, E.; Kilner, J. A. Tensile Lattice Distortion Does Not Affect Oxygen Transport in Yttria-Stabilized Zirconia−CeO_2 Heterointerfaces. *ACS Nano* **2012**, *6*, 10524−10534.
(23) Aydin, H.; Korte, C.; Rohnke, M.; Janek, J. Oxygen Tracer Diffusion Along Interfaces of Strained Y_2O_3/YSZ Multilayers. *Phys. Chem. Chem. Phys.* **2013**, *15*, 1944−1955.
(24) Lee, S.; Zhang, W.; Khatkhatay, F.; Jia, Q.; Wang, H.; MacManus-Driscoll, J. L. Strain Tuning and Strong Enhancement of Ionic Conductivity in $SrZrO_3$−RE_2O_3 (RE = Sm, Eu, Gd, Dy, and Er) Nanocomposite Films. *Adv. Funct. Mater.* **2015**, *25*, 4328−4333.
(25) Gaboriaud, R. J.; Pailloux, F.; Guerin, P.; Paumier, F. Yttrium Oxide Thin Films, Y_2O_3, Grown by Ion Beam Sputtering on Si. *J. Phys. D: Appl. Phys.* **2000**, *33*, 2884−2889.
(26) Wang, B.; Lewis, R. J.; Cormack, A. N. Computer Simulations of Large-scale Defect Clustering and Nanodomain Structure in Gadolinia-doped Ceria. *Acta Mater.* **2011**, *59*, 2035−2045.
(27) Schichtel, N.; Korte, C.; Hesse, D.; Janek, J. Elastic Strain at Interfaces and its Influence on Ionic Conductivity in Nanoscaled Solid Electrolyte Thin Films—Theoretical Considerations and Experimental Studies. *Phys. Chem. Chem. Phys.* **2009**, *11*, 3043−3048.
(28) Jhang, J. H.; Schaefer, A.; Cartas, W.; Epuri, S.; Bäumer, M.; Weaver, J. F. Growth and Partial Reduction of Sm_2O_3(111) Thin Films on Pt(111): Evidence for the Formation of SmO(100). *J. Phys. Chem. C* **2013**, *117*, 21396−21406.
(29) Guo, Q.; Zhao, Y.; Jiang, C.; Mao, W. L.; Wang, Z. Phase Transformation in Sm_2O_3 at High Pressure: In situ Synchrotron X-ray Diffraction Study and ab initio DFT Calculation. *Solid State Commun.* **2008**, *145*, 250−254.
(30) Shen, W.; Jiang, J.; Hertz, J. L. Beneficial Lattice Strain in Heterogeneously Doped Ceria. *J. Phys. Chem. C* **2014**, *118*, 22904−22912.
(31) Jiang, J.; Shen, W.; Hertz, J. L. Fabrication of Epitaxial Zirconia and Ceria Thin Films with Arbitrary Dopant and Host Atom Composition. *Thin Solid Films* **2012**, *522*, 66−70.
(32) Kim, H. R.; Kim, J. C.; Lee, K. R.; Ji, H. I.; Lee, H. W.; Lee, J. H.; Son, J. W. 'Illusional' Nano-size Effect Due To Artifacts of In-plane Conductivity Measurements of Ultra-Thin Films. *Phys. Chem. Chem. Phys.* **2011**, *13*, 6133−6137.
(33) Lee, K. R.; Ahn, K.; Chung, Y. C.; Lee, J. H.; Yoo, H. I. Lattice Distortion Effect on Electrical Properties of GDC Thin Films: Experimental Evidence and Computational Simulation. *Solid State Ionics* **2012**, *229*, 45−53.
(34) Steele, B. C. H. Appraisal of $Ce_{1-y}Gd_yO_{2-y/2}$ Electrolytes for IT-SOFC Operation at 500 °C. *Solid State Ionics* **2000**, *129*, 95−110.
(35) Mogensen, M.; Sammes, N. M.; Tompsett, G. A. Physical, Chemical and Electrochemical Properties of Pure and Doped Ceria. *Solid State Ionics* **2000**, *129*, 63−94.
(36) Korte, C.; Keppner, J.; Peters, A.; Schichtel, N.; Aydin, H.; Janek, J. Coherency Strain and its Effect on Ionic Conductivity and Diffusion in Solid Electrolytes − An Improved Model for Nanocrystalline Thin Films and a Review of Experimental Data. *Phys. Chem. Chem. Phys.* **2014**, *16*, 24575−24591.
(37) Schichtel, N.; Korte, C.; Hesse, D.; Zakharov, N.; Butz, B.; Gerthsen, D.; Janek, J. On the Influence of Strain on Ion Transport: Microstructure and Ionic Conductivity of Nanoscale YSZ| Sc_2O_3 Multilayers. *Phys. Chem. Chem. Phys.* **2010**, *12*, 14596−14608.
(38) Li, B.; Zhang, J.; Kaspar, T.; Shutthanandan, V.; Ewing, R. C.; Lian, J. Multilayered YSZ/GZO Gilms with Greatly Enhanced Ionic Conduction for Low Temperature Solid Oxide Fuel Cells. *Phys. Chem. Chem. Phys.* **2013**, *15*, 1296−1301.
(39) Aydin, H.; Korte, C.; Janek, J. ^{18}O-tracer Diffusion Along Nanoscaled Sc_2O_3/Yttria Stabilized Zirconia (YSZ) Multilayers: On the Influence of Strain. *Sci. Technol. Adv. Mater.* **2013**, *14*, No. 035007.
(40) Korte, C.; Schichtel, N.; Hesse, D.; Janek, J. Influence of Interface Structure on Mass Transport in Phase Boundaries between Different Ionic Materials. *Monatsh. Chem. Chem. Mon.* **2009**, *140*, 1069−1080.
(41) Karthikeyan, A.; Ramanathan, S. Temperature-dependent Interfacial Carrier Transport in Low-dimensional Oxides Using Ionic Conductor-insulator (YDZ-SiO_2) Superlattices. *J. Appl. Phys.* **2008**, *104*, No. 124314.
(42) Zhang, J.; Liang, E. J.; Sun, Q.; Jia, Y. Oxygen Vacancy Formation and Migration in Sr-and Mg-Doped $LaGaO_3$: A Density Functional Theory Study. *Chin. Phys. B* **2012**, *21*, No. 047201.
(43) Omar, S.; Wachsman, E. D.; Jones, J. L.; Nino, J. C. Crystal Structure−Ionic Conductivity Relationships in Doped Ceria Systems. *J. Am. Ceram. Soc.* **2009**, *92*, 2674−2681.
(44) Dholabhai, P. P.; Adams, J. B.; Crozier, P.; Sharma, R. A Density Functional Study of Defect Migration in Gadolinium Doped Ceria. *Phys. Chem. Chem. Phys.* **2010**, *12*, 7904−7910.
(45) Ahn, K.; Chung, Y. C.; Yoon, K. J.; Son, J. W.; Kim, B. K.; Lee, H. W.; Lee, J. H. Lattice-Strain Effect on Oxygen Vacancy Formation in Gadolinium-Doped Ceria. *J. Electroceram.* **2014**, *32*, 72−77.
(46) Hinterberg, J.; Zacherle, T.; De Souza, R. A. Activation Volume Tensor for Oxygen-Vacancy Migration in Strained CeO_2 Electrolytes. *Phys. Rev. Lett.* **2013**, *110*, No. 205901.
(47) Azad, S.; Marina, O. A.; Wang, C. M.; Saraf, L.; Shutthanandan, V.; McCready, D. E.; El-Azab, A.; Jaffe, J. E.; Engelhard, M. H.; Peden, C. H. F.; Thevuthasan, S. Nanoscale Effects on Ion Conductance of Layer-by-Layer Structures of Gadolinia-Doped Ceria and Zirconia. *Appl. Phys. Lett.* **2005**, *86*, No. 131906.
(48) Peters, A.; Korte, C.; Hesse, D.; Zakharov, N.; Janek, J. Ionic Conductivity and Activation Energy for Oxygen Ion Transport in Superlattices—The Multilayer System CSZ (ZrO_2+ CaO)/Al_2O_3. *Solid State Ionics* **2007**, *178*, 67−76.
(49) Ohtomo, A.; Hwang, H. Y. A High-Mobility Electron Gas at the $LaAlO_3$/$SrTiO_3$ Heterointerface. *Nature* **2004**, *427*, 423−426.
(50) Bousquet, E.; Dawber, M.; Stucki, N.; Lichtensteiger, C.; Hermet, P.; Gariglio, S.; Triscone, J. M.; Ghosez, P. Improper Ferroelectricity in Perovskite Oxide Artificial Superlattices. *Nature* **2008**, *452*, 732−736.
(51) Okamoto, S.; Millis, A. J. Electronic Reconstruction at an Interface between a Mott Insulator and a Band Insulator. *Nature* **2004**, *428*, 630−633.
(52) Mannhart, J.; Schlom, D. G. Oxide Interfaces—An Opportunity for Electronics. *Science* **2010**, *327*, 1607−1611.
(53) Chakhalian, J.; Freeland, J. W.; Srajer, G.; Strempfer, J.; Khaliullin, G.; Cezar, J. C.; Charlton, T.; Dalgliesh, R.; Bernhard, C.; Cristiani, G.; Habermeier, H.-U.; Keimer, B. Magnetism at the

https://doi.org/10.1021/acsaelm.3c00724
ACS Appl. Electron. Mater. 2023, 5, 4556−4563

Interface between Ferromagnetic and Superconducting Oxides. *Nat. Phys.* **2006**, *2*, 244−248.
(54) Tokura, Y.; Nagaosa, N. Orbital Physics in Transition-Metal Oxides. *Science* **2000**, *288*, 462−468.
(55) Shen, W.; Hertz, J. L. Ionic Conductivity of YSZ/CZO Multilayers with Variable Lattice Mismatch. *J. Mater. Chem. A* **2015**, *3*, 2378−2386.
(56) Baiutti, F.; Chiabrera, F.; Acosta, M.; Diercks, D.; Parfitt, D.; Santiso, J.; Wang, X.; Cavallaro, A.; Morata, A.; Wang, H.; Chroneos, A.; MacManus-Driscoll, J.; Tarancon, A. A High-Entropy Manganite in an Ordered Nanocomposite for Long-Term Application in Solid Oxide Cells. *Nat. Commun.* **2021**, *12*, No. 2660.
(57) Huang, H.; Gür, T. M.; Saito, Y.; Prinz, F. High Ionic Conductivity in Ultrathin Nanocrystalline Gadolinia-Doped Ceria Films. *Appl. Phys. Lett.* **2006**, *89*, No. 143107.
(58) Tsuchiya, M.; Bojarczuk, N. A.; Ramanathan, S. Molecular Beam Synthesis and High Temperature Electrical Properties of Crystalline Ceria Thin Films. *Appl. Phys. Lett.* **2007**, *91*, No. 223101.
(59) Bishop, S. R.; Duncan, K. L.; Wachsman, E. D. Surface and Bulk Oxygen Non-stoichiometry and Bulk Chemical Expansion in Gadolinium-doped Cerium Oxide. *Acta Mater.* **2009**, *57*, 3596−3605.
(60) Tietz, F. Thermal Expansion of SOFC Materials. *Ionics* **1999**, *5*, 129−139.
(61) Sediva, E.; Bohdanov, D.; Harrington, G. F.; Rafalovskyi, I.; Drahokoupil, J.; Borodavka, F.; Marton, P.; Hlinka, J. Anisotropic Strain in Rare-Earth Substituted Ceria Thin Films Probed by Polarized Raman Spectroscopy and First-Principles Calculations. *ACS Appl. Mater. Interfaces* **2020**, *12*, 56251−56259.
(62) Acharya, S. A.; Gaikwad, V. M.; D'Souza, S. W.; Barman, S. R. Gd/Sm Dopant-Modified Oxidation State and Defect Generation in Nano-Ceria. *Solid State Ionics* **2014**, *260*, 21−29.

https://doi.org/10.1021/acsaelm.3c00724
ACS Appl. Electron. Mater. 2023, 5, 4556−4563